Title
Gene expression tomography

Journal
Physiological Genomics, 8(2)

ISSN
1094-8341

Authors
BROWN, VANESSA M
OSSADTCHI, ALEX
KHAN, ARSHAD H
et al.

Publication Date
2002-02-28

DOI
10.1152/physiolgenomics.00090.2001

Gene expression tomography

Vanessa M. Brown,[1,2] Alex Ossadtchi,[3] Arshad H. Khan,[1,2]

Sanjiv S. Gambhir,[1,2,4,5,6] Simon R. Cherry, [1,2,4,5,6,7]

Richard M. Leahy,[3] Desmond J. Smith,[1,2,4,5,6]

[1] Department of Molecular and Medical Pharmacology,
[2] Crump Institute for Molecular Imaging,
[4] University of California/Department of Energy Laboratory of Structural and Biology and Molecular Medicine,
[5] Brain Research Institute,
[6] Jonsson Comprehensive Cancer Center,
School of Medicine,
University of California,
Los Angeles, CA 90095

[3] Department of Electrical Engineering,
Signal and Image Processing Institute,
School of Engineering,
University of Southern California,
Los Angeles, CA 90089

[7] Present address:
Department of Biomedical Engineering,
One Shields Ave,
University of California,
Davis, CA 95616

Running title: Gene expression tomography

Address for reprint requests and other correspondence: D.J. Smith, Dept Pharmacology, UCLA School of Medicine, 23-120 CHS, Box 951735, Los Angeles, CA 90095-1735; Tel: (310) 206-0086, Fax: (310) 825-6267; E-mail: DSmith@mednet.ucla.edu

Gene expression tomography, or GET, is a new method to increase the speed of 3D gene expression analysis in the brain. The name is evocative of the method's dual foundations in high throughput gene expression analysis and computerized tomographic image reconstruction, familiar from techniques such as PET and CT. In GET, brain slices are taken using a cryostat in conjunction with axial rotation about independent axes to create a series of "views" of the brain. Gene expression information obtained from the axially rotated views can then be used to recreate 3D gene expression patterns. GET was used to successfully reconstruct images of tyrosine hydroxylase gene expression in the mouse brain, using both RNase protection and real-time QRT-PCR. A Monte-Carlo analysis confirmed the good quality of the GET image reconstruction. By speeding acquisition of gene expression patterns, GET may help improve our understanding of the genomics of the brain in both health and disease.

brain mapping, genomics, real-time QRT-PCR, RNase protection, tomographic image reconstruction

Comprehensive acquisition of gene expression patterns will be an important approach to understanding how the genome constructs the brain. The resulting information will allow the genetic logic underlying the development of the brain to be deciphered by (i) providing the gene expression "signatures" that direct differentiation of various brain regions (ii) allowing identification of the genes induced and repressed in disorders affecting the brain (iii) permitting elucidation of networks of co-regulated genes and their relevant *cis*-acting regulatory sequences by seeking co-ordinate expression patterns (space and time) that result from variations due to anatomy, development, disease, environment and genetic polymorphism.

The recent development of high throughput multiplex gene expression methodologies, including microarrays (2), gene chips (11), and SAGE (19) have given important insights into gene networks in unicellular systems. However, these methods have yet to be employed to analyze how the genome constructs the three dimensional (3D) structure of multicellular organisms. Classical approaches to gene expression in the brain, such as *in situ* hybridization and autoradiography, can be employed to obtain series of 2D gene expression patterns, which are stackable for provision of 3D images. However, such methods are difficult to adapt to high throughput. In living animals, techniques exist for 3D imaging of gene expression, but these methods also lack high throughput capability (7, 10, 12, 21). Here, the feasibility of a method called gene expression tomography (GET) is demonstrated. GET employs the image

reconstruction methodologies of biomedical imaging systems, such as CT and PET, to produce volumetric maps of gene expression, in principle in high throughput. GET was employed to reconstruct the expression pattern of the tyrosine hydroxylase (TH) gene in the brain, using quantification based on both RNase protection and real-time quantitative reverse transcription PCR (QRT-PCR). The TH gene is expressed in a number of brain regions, including the periventricular/paraventricular nuclei, zona incerta, substantia nigra, ventral tegmental area, median raphe nucleus and locus coeruleus (13, 17). GET resulted in images that correctly depicted the prominent features of TH gene expression. In addition, a statistical approach to image quantification demonstrated the high quality and reproducibility of the GET reconstructions when compared to the known TH expression pattern.

MATERIALS AND METHODS

β-galactosidase staining. The transgenic mouse line TH9.0-16 was employed (13). These mice harbor a transgene consisting of 9.0 kb of 5' upstream sequence from the rat TH gene fused to the E. coli lacZ reporter gene. The expression pattern of the reporter recapitulates the known pattern of the TH gene. Brains were prepared for β-galactosidase staining as follows (13). Transgenic mice and non-transgenic sibling controls were anesthetized with 2.5% Avertin, perfused transcardially with saline containing 0.5% $NaNO_2$ and 10 U ml^{-1} heparin, followed by fixative (0.5% paraformaldehyde, 2% glutaraldehyde in 0.1 M phosphate buffer, pH 7.4). Brains were removed with the olfactory bulbs

left behind, post-fixed for 30-45 min, rinsed in phosphate buffer and cryoprotected in 30% sucrose. Coronal sections of 40 μm were obtained using a cryomicrotome and incubated overnight in 3.1 mM $K_3Fe(CN)_6$, 3.1 mM $K_4Fe(CN)_6$, 0.15 M NaCl, 1 mM $MgCl_2$, 0.01% sodium deoxycholate, 0.02% NP-40, 0.2 mg ml^{-1} X-gal in 10 mM phosphate buffer (pH 7.4). When the color had developed, sections were counterstained with nuclear fast red and coverslipped using Permount. To simplify comparison of the β-galactosidase staining with the GET reconstructions, the lacZ images were transformed into pseudocolor and warped onto corresponding sections of the mouse brain atlas (14, 20). The warping was accomplished using our own implementation (web site below) of the thin-plate splines warping method (1).

Acquisition of slices for GET. Eight week old male C57BL/6J mice were euthanized by overdose with halothane, and their brains removed with the olfactory bulbs left behind. The brains were frozen, embedded in tissue freezing medium (Triangle Biomedical Sciences, Durham, N.C.), and parallel slices obtained using a cryostat. Each set of parallel slices from one specimen is called a “view”. For each view, aggregate slices of 1 mm were obtained by pooling 17 cryostat slices of 60 μm. The specimen was oriented in the cryostat at the angles described below using the interhemispheric fissure as a reproducible landmark. Using a right-handed co-ordinate system, the three axes of rotation were x: posterior to anterior, y: left to right, z inferior to superior (Fig. 1). Three views were obtained per axis of rotation, -45°, 0°, and +45°, with a right-handed rotation

about each axis. A total of nine views was hence acquired (three axes of rotation multiplied by three views per axis). For the x axis of rotation, the 0° view corresponded to the x-y plane (parallel transverse slices), for the y axis, the y-z plane (parallel coronal slices), and for the z axis, the z-x plane (parallel sagittal slices). Multiple experiments showed remarkable uniformity of slice acquisition from one sample to the next for a particular view. This is consistent with data showing that mice of the same age from inbred strains such as C57BL/6J have minimal interindividual variation in brain morphology (20).

RNA extraction. Total RNA was extracted from the aggregate slices using Trizol reagent (GibcoBRL), following the manufacturer's instructions. Briefly, tissue was homogenized in Trizol (1 ml of reagent per 50 mg of tissue) and centrifuged at 12,000 g for 10 minutes. The supernatant was incubated at room temperature for 5 min and 0.2 ml of chloroform added per ml Trizol. The mixture was shaken vigorously for 15 s, incubated at room temperature for 3 min, and centrifuged at 12,000 g for 15 min. RNA was precipitated from the supernatant by adding 0.5 ml isopropyl alcohol per ml Trizol, incubating at room temperature for 10 min, and centrifuging at 12,000 g for 10 min. The RNA pellet was washed once with 75% ethanol, air dried, and dissolved in water. Quantitation employed fluorometry, and the RNA yield per slice (mean ± SEM) was 51.1 μg ± 2.5.

RNase protection. RNase protection was performed as described (15). A probe of 349 nt hybridizing to sequences 816 to 1043 of the tyrosine hydroxylase (TH)

gene was employed, giving a protected fragment of 227 nt. Riboprobes were labeled with ^{32}P using Ambion's MAXIscript In Vitro Transcription Kit. From each 1 mm aggregate slice of brain tissue, 10 μg of total RNA was employed for the protection assay, following the manufacturer's instructions. The protected bands were quantitated by scanning and densitometry using NIH Image, version 1.61. Each sample's densitometry measurement was normalized using mouse whole brain control, so that the relative ratio of each sample could be compared across experiments. However, because of finite sampling, additional computational normalization was required for image reconstruction, which was achieved by equalizing the peak expression level in each view.

Real-time quantitative reverse transcription polymerase chain reaction. Real-time quantitative reverse transcription polymerase chain reaction (QRT-PCR) employed TaqMan technology on an ABI Prism 7700 Sequence Detector (6, 8, 9). Reverse transcription was primed with oligo$[dT]_{12-18}$, and used 100 ng total RNA and Taqman reverse transcription reagents (Applied Biosystems), following the manufacturer's instructions. After reverse transcription, the amount of cDNA was quantitated using fluorometry, and 1 ng of cDNA employed in each real-time assay. The amplification primers specific for TH were 5'-TGTTGGCTGACCGCACAT-3' and 5'-AAGCCCCCAGAGATGCAAG-3', and the reporter oligonucleotide 5'-TGCCCAGTTCTCCCAGGACATTGG-3'. The 5' reporter dye was FAM, and the 3' quencher TAMRA. The amplification primers were at 200 nM and the reporter at 100 nM. A passive reference dye (ROX)

provided an internal standard for normalization of FAM fluorescence, correcting for fluctuations due to volume changes. Quantitation employed an external calibration curve constructed using the TH primers and reporter oligonucleotide together with known amounts of total brain cDNA. The TH forward and reverse primer set flanks intron 9, while the reporter oligonucleotide hybridizes across this intron site in the transcript. Consequently, genomic DNA artifacts are very unlikely. Nevertheless, the possibility of genomic contamination was further excluded by the use of no reverse transcriptase controls in combination with the TH forward and reverse primers. The samples were also analyzed using primers which cross the intron of the housekeeping gene GdX (16). All real time QRT-PCR experiments were performed in triplicate.

Image reconstruction. The GET imaging procedure employed filtered backprojection, as described (4, 18), but with modifications. The reconstructions were based on the planar integral projection reconstruction technique. For the purposes of the following discussion, the notion of a view corresponds to that of a projection in accepted tomography terms. Formally, each view (projection) can be defined by the pair of polar and azimuthal angles (θ,φ). Hence, each projection $p_{\theta,\varphi}(t)$ is given by the following integral:

$$p_{\theta,\varphi}(t) = \iiint_V G(x,y,z)\delta(t-T)dxdyxz \qquad (1)$$

where the direction T is defined as $T = x\cos\varphi\sin\theta + y\sin\varphi\ \sin\theta + z\cos\theta$. The expression is based on the sifting property of Dirac delta function (3). Dispersion functions other than the delta function could be employed, and might represent an attractive approach to a Bayesian formulation of GET, allowing additional sources of information (e.g. anatomy) to be taken into account when reconstructing gene expression images. Taking Fourier transforms of both sides of equation (1) we obtain:

$$
\begin{aligned}
&P_{\theta,\varphi}(\rho) = \int_{-\infty}^{\infty} p_{\theta,\varphi}(t)\exp(-i\rho t)dt = \int_{-\infty}^{\infty}\iiint_V g(x,y,z)\delta(t-T)dxdyxz\exp(-i\rho t)dt = \\
&= \iiint_V g(x,y,z)\exp\left(-i\rho\left(x\cos\varphi\sin\theta + y\sin\varphi\ \sin\theta + z\cos\theta\right)\right)dxdyxz = \qquad (2)\\
&= \iiint_V g(x,y,z)\exp\left(-i\left(x\rho_x(\theta,\varphi) + y\rho_y(\theta,\varphi) + z\rho_z(\theta,\varphi)\right)\right)dxdyxz = G(\omega_x,\omega_y,\omega_z)\,|_{\theta,\varphi}
\end{aligned}
$$

The result of equation (2) can be restated as follows: the "1-D Fourier transform of the planar-integral data at a given polar angle θ and azimuthal angle φ gives the 1-D radial frequency data in 3-D Fourier space $G(\omega_x,\omega_y,\omega_z)$".

Equation (2) gives one of the possible recipes for image reconstruction from the planar integral data. The first step of the method is based on interpolation in the frequency domain of the values of 1-D Fourier transform to obtain a Cartesian grid of Fourier transform values for the underlying image. The second step requires taking the inverse Fourier transform of the interpolated 3-D grid resulting in an estimate of the underlying gene expression image.

The values of polar angle θ and azimuthal angle φ are shown in Table 1. For each projection defined by the pair of angles (θ,φ), nine to twelve slices were acquired and the planar integrals of gene expression measured using RNase protection or real-time QRT-PCR. This constituted a set of discrete projections $p_{\theta,\varphi}(t_i)$, *i=1:12* for all pairs of angles listed in the table. The discrete Fourier transform was taken and the approximately 90 values on the polar grid were interpolated using the Gaussian kernel to obtain an estimate of the 3-D Fourier transform of the underlying image of the gene expression, $G(\omega_x,\omega_y,\omega_z)$. The actual image was reconstructed by simply computing the inverse Fourier transform, i.e. $\hat{g}(x,y,z)=F^{-1}\left(G\left(\omega_x,\omega_y,\omega_z\right)\right)$. Image registration was performed using the Mouse Brain Library (14, 20), and a widely employed atlas (5). For the purposes of presentation, C57BL/6J brain coronal sections from the Mouse Brain Library (14, 20) were employed.

Monte-Carlo analysis. The TH lacZ, RNase protection and real-time QRT-PCR GET images were reduced to binary 12 x 12 pixel arrays. Random images consisted of the 12 x 12 pixel arrays permuted according to binomial statistics, with the expected number of active pixels equivalent to those obtained from the experimental images. To assess the similarity between distributions, the Tanimoto coefficient (area of intersection between distributions/union area of the distributions) was employed. A total of 10,000 permutations was employed for each comparison.

Web site. The algorithms and study results are available on a web site (www.pharmacology.ucla.edu/smithlab/physiolgenomics_supp).

RESULTS

Principles underlying GET. GET involves taking sets of parallel brain slices acquired from several samples by incremental tilting about multiple axes of rotation (Fig. 1). Because of the two-fold symmetry of the parallel slices, a rotation of 180° about each axis is sufficient for a complete data set. Each set of parallel slices is called a "view" of the brain. Gene expression information obtained from the axially rotated views is employed in image reconstruction algorithms similar to those employed in biomedical imaging technologies, such as CT and PET, allowing computerized reconstruction of 3D gene expression patterns. By analogy with CT and PET, each of the sets of parallel slices in GET represents a projection image of the gene expression profile from the relevant view. The total number of voxels that can be obtained from the reconstruction equals the number of samples analyzed, and hence the expected voxel number, Vx, = A.V.S, where A = the number of axes of rotation, V = the number of views per axis, and S = the number of slices per view. The anticipated volumetric resolution of the reconstructed image is given by the volume of the mouse brain (approximately 300 μl), divided by the number of voxels. GET is modality independent, and any gene expression analysis method can be used, depending on requirements of reproducibility, throughput and sensitivity.

Reconstructing the TH gene expression pattern using GET and RNase protection. TH is the rate limiting enzyme in catecholamine biosynthesis, including synthesis of dopamine. The expression pattern of the TH gene is shown in Fig. 2A, using staining for β-galactosidase activity in a line of lacZ transgenic mice that faithfully reproduces the expression pattern of the gene (13). The TH gene is strongly expressed in a number of dopamine producing cell groups located in the ventral mesencephalon, including the ventral tegmental area, which gives rise to the mesolimbic and mesocortical dopamine pathways, and the substantia nigra which gives rise to the nigrostriatal pathway (13, 17). The gene is also expressed in the hypothalamus (peri/paraventricular nuclei), zona incerta, median raphe nucleus and locus coeruleus. The TH gene expression images were transformed into pseudocolor and warped onto corresponding sections of the mouse brain atlas (14, 20) (Fig. 2B) in order to facilitate comparison with reconstructions obtained using GET.

To image TH gene expression, a GET experiment was performed using three orthogonal axes of rotation, and three equally spaced views per axis (+45°, 0°, -45°) (Fig. 1). At 0°, the three axes represented transverse, coronal and sagittal sections. For each view, aggregate slices of 1 mm were taken using the cryostat, giving approximately 10 slices per view (mean ± SEM, 10.1 ± 0.3; range 9 to 11). TH transcript levels were quantitated using RNase protection analysis of equal amounts of RNA (10 μg) from each slice (Fig. 3). The TH gene expression images reconstructed from this data using GET and filtered backprojection are

shown in Fig. 4. Within the expected limits of resolution (below), the reconstructed image is highly similar to the known expression pattern of the TH gene, with the most prominent expression being in the midbrain (substantia nigra and ventral tegmental area), ventral diencephalon (periventricular/paraventricular hypothalamic nuclei, zona incerta) and pons (locus coeruleus) (13, 17). Ectopic areas of reconstructed expression were also present; most notably, expression in the ventral tegmental area appeared to be duplicated dorsally.

Since the total number of voxels from a tomographic image reconstruction equals the number of analyzed samples (Vx = A.V.S.), and approximately 90 samples were analyzed in this GET reconstruction (3 axes of rotation x 3 views per axis x 10.1 slices per view), a 90 voxel reconstruction is expected. The anticipated volumetric resolution is given by the volume of the mouse brain (300 μl), divided by the number of voxels (90), and is approximately 3 μl, equivalent to a linear resolution of 1.5 mm. It was expected that this level of resolution would be sufficient to image bilaterally symmetric parasagittal midline structures, and this expectation was clearly borne out (Fig. 4), where it was possible to resolve the left and right locus coeruleus, zona incerta and substantia nigra.

Reconstructing the TH gene expression pattern using GET and real-time QRT-PCR. To investigate the modality independence of GET, and to explore its potential for higher resolution in the context of a more sensitive analytic technique, the expression pattern of the TH gene was reconstructed using real-

time QRT-PCR. The reconstruction scheme employed three axes of rotation and three views per axis, as described above, with an aggregate slice thickness from the cryostat of 1 mm. The mean (± SEM) number of slices per view was 11.1 ± 0.3, range 10-12. The results of the real-time QRT-PCR are shown in Fig. 5, and the results of the reconstruction in Fig. 6. The reconstructed TH gene expression image again replicated the major features of the known pattern, with expression observed in the substantia nigra, ventral tegmental area, peri/paraventricular hypothalamic nuclei, zona incerta and locus coeruleus. However, some aberrations were present, including dorsally shifted expression for the ventral tegmental area and bilaterally symmetric splitting of expression for the peri/paraventricular nuclei in anterior-most sections.

Quantitative analysis of GET image reconstruction quality. To assess how well GET had reconstructed the expression pattern of the TH gene, a Monte-Carlo analysis was performed. The pseudocolor TH lacZ, RNase protection and real-time QRT-PCR GET images were reduced to binary 12 x 12 pixel arrays. These images were compared to random images consisting of the 12 x 12 pixel arrays permuted according to binomial statistics, with the expected number of active pixels equivalent to those obtained from the experimental images. A total of 10,000 permutations was employed for each comparison. To assess the similarity between distributions, the Tanimoto coefficient (area of intersection between distributions/union area of the distributions) was employed. Both the RNase protection and the real-time QRT-PCR GET images were statistically

more similar to the lacZ TH images than to random images ($p = 0.0068$ for both comparisons). In addition, there was no statistical difference between the two sets of GET images ($p = 0.1$), suggesting good internal consistency.

DISCUSSION

The present studies demonstrate that tomographic approaches can be used to reconstruct 3D images of gene expression. Within the anticipated limits of resolution, the GET images were shown to reproduce the major features of TH gene expression. The TH gene is strongly expressed in dopaminergic neurons located in the ventral mesencephalon, including the ventral tegmental area, which gives rise to the mesolimbic and mesocortical dopamine pathways, and the substantia nigra which gives rise to the nigrostriatal pathway (13, 17). The gene is also expressed in the hypothalamus (paraventricular/periventricular nuclei), zona incerta, median raphe nucleus and the locus coeruleus (13). Using GET, TH expression was detected in all regions expected, although anomalies were noted relating to the ventral tegmental area and the peri/paraventricular nuclei. Part of these discrepancies may be explained by the fact that the lacZ images of TH gene expression represented images from staining of 40 μm sections, whereas the GET images represented 1 mm slices, with consequent averaging of expression patterns across anatomical structures. A Monte-Carlo analysis of the TH gene expression images obtained from GET revealed good fidelity when compared with the known expression pattern.

A potential advantage of GET is that it transforms the complex 3D anatomy of the brain into arrays of biochemical samples, providing valuable opportunities for scalability and automatability, and hence high throughput. These attributes are difficult to obtain with classical techniques such as *in situ* hybridization. GET requires multiple samples for successful image reconstruction, and the high degree of interindividual uniformity of brains from inbred mice (5, 20) is a significant advantage, allowing simple registration of images. However, in situations where there is a higher degree of variation, such as brains from humans, rats or other outbred organisms, the use of warping software to allow computational image registration (4, 18) should permit GET to be employed. This image registration will be facilitated by the use of "reference" genes, whose expression patterns are well documented and which together cover the entire brain. Although GET requires multiple samples, the high sensitivity of modern gene expression technologies should allow GET to acquire a large number of gene expression patterns from only a limited number of brains. This is an advantage compared to *in situ* hybridization, which generally requires a new brain for analysis of each gene. The resolution of GET scales with the number of axes of rotation, the number of views per axis, and the number of slices per view. Thus, in principle, the resolution of the method is limited only by the sensitivity of the gene expression methodology employed. Using real-time QRT-PCR, sufficient RNA should be obtainable from slices of the mouse brain to allow a resolution as high as 10 μm.

GET is modality independent, and the technology may be useful for analysis of the transcriptome, the proteome or reporter genes such as green fluorescent protein. Another possibility is the use of voltage-sensitive dyes for analysis of samples (either as slices or dissociated cells) combined with tomographic image reconstruction, perhaps allowing three dimensional insights into electrophysiology. In the realm of gene expression, the high throughput acquisition of expression patterns using GET may be useful in identifying abnormal brain regions in disorders where, despite years of study, the responsible areas are still unclear e.g. schizophrenia and Down syndrome. In sum, GET should be a useful approach to better understanding of the genomics of the brain and its disorders.

Supported by grants from the Dana Foundation, Merck Genome Research Institute, W.M. Keck Foundation, National Foundation for Functional Brain Imaging, NIH, NSF, Staglin Music Festival and NARSAD Young Investigator Award, and UCLA School of Medicine.

REFERENCES

1. **Bookstein FL.** Principal warps: thin-plate splines and the decomposition of deformations. *IEEE Transactions on Pattern Analysis and Machine Intelligence* 11: 567-585, 1989.
2. **Brown PO, and Botstein D.** Exploring the new world of the genome with DNA microarrays. *Nat Genet* 21: 33-37, 1999.
3. **Cho ZH, Singh M, and Jones JP.** *Foundations of medical imaging*. New York: Wiley, 1993.
4. **Frackowiak RSJ, Friston KJ, Frith CD, Dolan RJ, and Mazziotta JC.** *Human Brain Function*. London, UK: Academic Press Ltd, 1997.
5. **Franklin KBJ, and Paxinos G.** *The mouse brain in stereotaxic coordinates*. San Diego: Academic Press, 1997.
6. **Freeman WM, Walker SJ, and Vrana KE.** Quantitative RT-PCR: pitfalls and potential. *BioTechniques* 26: 112-125, 1999.
7. **Gambhir SS, Barrio JR, Herschman HR, and Phelps ME.** Assays for noninvasive imaging of reporter gene expression. *Nucl Med Biol* 26: 481-490, 1999.
8. **Gibson UE, Heid CA, and Williams PM.** A novel method for real time quantitative RT-PCR. *Genome Res* 6: 995-1001, 1996.
9. **Heid CA, Stevens J, Livak KJ, and Williams PM.** Real time quantitative PCR. *Genome Res* 6: 986-994, 1996.
10. **Herschman HR, MacLaren DC, Iyer M, Namavari M, Bobinski K, Green LA, Wu L, Berk AJ, Toyokuni T, Barrio JR, Cherry SR, Phelps ME,**

Sandgren EP, and Gambhir SS. Seeing is believing: non-invasive, quantitative and repetitive imaging of reporter gene expression in living animals, using positron emission tomography. *J Neurosci Res* 59: 699-705, 2000.

11. **Lipshutz RJ, Fodor SP, Gingeras TR, and Lockhart DJ.** High density synthetic oligonucleotide arrays. *Nat Genet* 21: 20-24, 1999.
12. **Louie AY, Hüber MM, Ahrens ET, Rothbächer U, Moats R, Jacobs RE, Fraser SE, and Meade TJ.** In vivo visualization of gene expression using magnetic resonance imaging. *Nat Biotechnol* 18: 321-325, 2000.
13. **Min N, Joh TH, Kim KS, Peng C, and Son JH.** 5' upstream DNA sequence of the rat tyrosine hydroxylase gene directs high-level and tissue-specific expression to catecholaminergic neurons in the central nervous system of transgenic mice. *Brain Res Mol Brain Res* 27: 281-289, 1994.
14. **Rosen GD, Williams AG, Capra JA, Connolly MT, Cruz B, Lu L, Airey DC, Kulkarni K, and Williams RW.** The Mouse Brain Library @ www.mbl.org. *Int Mouse Genome Conference* 14: 166. www.mbl.org., 2000.
15. **Sambrook J, Maniatis T, and Fritsch EF.** *Molecular cloning : a laboratory manual*. Cold Spring Harbor, N.Y.: Cold Spring Harbor Laboratory, 1989.
16. **Smith DJ, Stevens ME, Sudanagunta SP, Bronson RT, Makhinson M, Watabe AM, O'Dell TJ, Fung J, Weier HU, Cheng JF, and Rubin EM.** Functional screening of 2 Mb of human chromosome 21q22.2 in transgenic mice implicates minibrain in learning defects associated with Down syndrome. *Nat Genet* 16: 28-36, 1997.

17. **Stork O, Hashimoto T, and Obata K.** Haloperidol activates tyrosine hydroxylase gene-expression in the rat substantia nigra, pars reticulata. *Brain Res* 633: 213-222, 1994.

18. **Toga AW, and Mazziotta JC.** *Brain mapping : the methods*. San Diego: Academic Press, 1996.

19. **Velculescu VE, Zhang L, Vogelstein B, and Kinzler KW.** Serial analysis of gene expression. *Science* 270: 484-487, 1995.

20. **Williams RW.** Mapping genes that modulate mouse brain development: a quantitative genetic approach. In: *Mouse Brain Development*, edited by A. F. Goffinet and P. Rakic. New York: Springer, 2000, p. 21–49.

21. **Zacharias DA, Baird GS, and Tsien RY.** Recent advances in technology for measuring and manipulating cell signals. *Curr Opin Neurobiol* 10: 416-421, 2000.

Fig. 1. Principles underlying GET. **(A)** A rotated series of "views" through independent axes provides sets of parallel slices for gene expression analysis. Shown is the right handed co-ordinate system and three orthogonal axes x, y and z employed for acquisition of the views. Right handed rotation about each axis was employed to obtain three equally spaced views at +45°, 0°, and –45°. For the x axis of rotation, the 0° view corresponded to the x-y plane (parallel transverse slices), for the y axis, the y-z plane (parallel coronal slices), and for the z axis, the z-x plane (parallel sagittal slices). The figure shows the 0° view of the z axis (sagittal slices). Any gene expression analysis method can be used, depending on requirements of reproducibility, throughput and sensitivity. **(B)** The three views for each axis of rotation. Each of the x, y and z axes are depicted, looking from the positive towards the negative co-ordinates of each axis. For each view at +45°, 0°, and –45°, roughly ten parallel slices were harvested.

Fig. 2. Expression pattern of the TH gene. **(A)** Coronal brain sections from mice expressing lacZ in the authentic expression pattern of the TH gene. The sections have been stained for β-galactosidase activity. IA, interaural; Br, bregma. Sections of the mouse brain are shown at approximately 0.8 mm intervals (mean ± SEM for both IA and Br: 0.83 ± 0.14) proceeding (left to right, up to down) from IA +4.18 mm, Br -0.38 mm to IA -1.66 mm, Br –5.46 mm (5, 14, 20). **(B)** TH gene expression pattern warped onto mouse brain atlas sections (14, 20). The level of expression is shown using a pseudocolor scale. Periventricular/paraventricular hypothalamic nuclei, Pe/Pa; zona incerta, ZI; substantia nigra, SN; ventral tegmental area, VTA; median raphe nucleus, MnR; locus coeruleus, LC.

Fig. 3. RNase protection assays for TH. **(A)** Results of RNase protection assay for one view (x axis, +45 degrees), showing the protected fragment of 227 nt. The reference signal from whole brain is shown in lane r. **(B)** Quantitation of TH levels for all views. A relative expression scale is employed, in which the units employed are arbitrary. On this relative scale the expression level of the whole brain reference is less than one (about 0.3 for x axis, +45°). Because of finite sampling, further normalization was required for the image reconstruction (Fig. 4), and in order to achieve this, the peak expression in each view was equalized (Materials and Methods).

Fig. 4. GET image reconstruction of TH gene expression using RNase protection data. Coronal sections of the mouse brain are shown as for Fig. 2B. TH expression was detected in all regions expected, although some anomalies were noted, including dorsally duplicated expression for the VTA.

Fig. 5. Real-time QRT-PCR for TH. All reactions were performed in triplicate. Mean expression values ± SEM are shown, except error bars are sometimes too small to be visible. A relative scale was employed, as for Fig. 3B.

Fig. 6. GET image reconstruction of TH gene expression using real-time QRT-PCR data. Coronal sections of the mouse brain are shown as for Fig. 2B. TH expression was detected in all regions expected, although some anomalies were noted, including dorsally shifted expression for the VTA, and bilaterally symmetric splitting of expression for the peri/paraventricular nuclei in anterior-most sections.

Table 1. Values of polar angle θ and azimuthal angle φ

axis angle	x		y		z	
	θ	φ	θ	φ	θ	φ
+45	-135	90	-45	0	90	-45
0	180	N/A	90	0	90	-90
-45	135	-90	-135	0	90	135

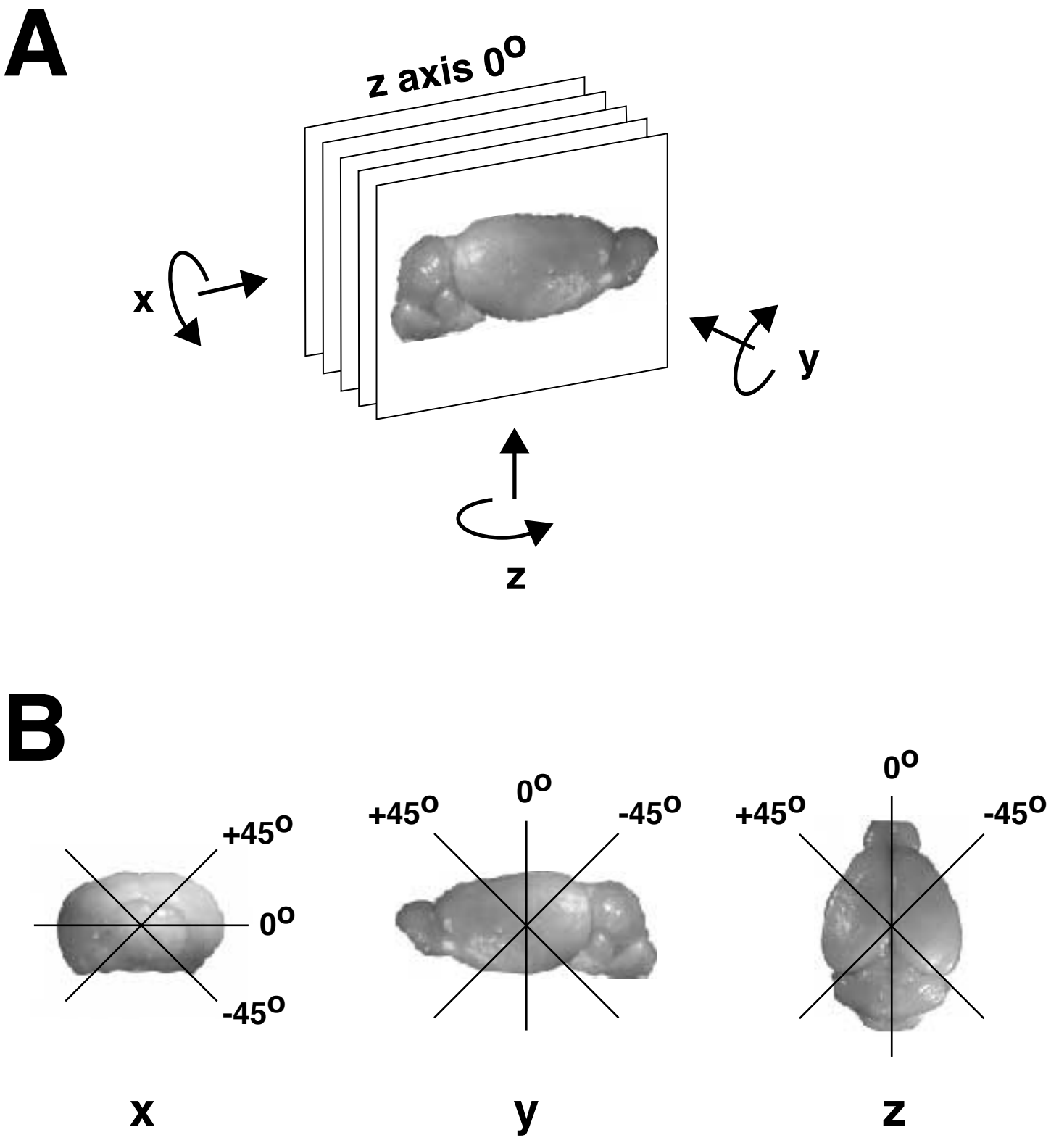

Fig. 1

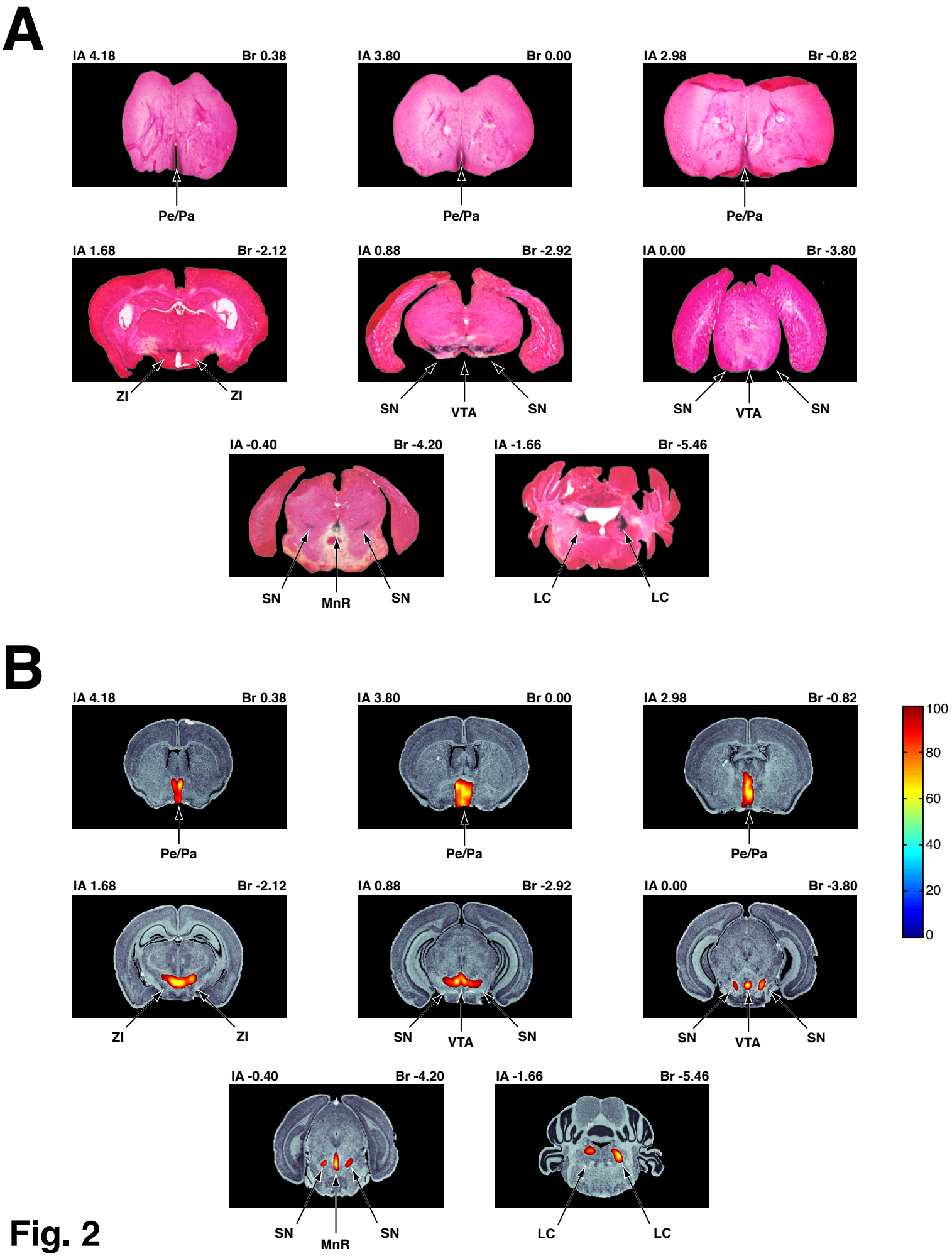
A
IA 4.18
Br 0.38
Pe/Pa
IA 3.80
Br 0.00
Pe/Pa
IA 2.98
Br -0.82
Pe/Pa
IA 1.68
Br -2.12
ZI
ZI
IA 0.88
Br -2.92
SN
VTA
SN
IA 0.00
Br -3.80
SN
VTA
SN
IA -0.40
Br -4.20
SN
MnR
SN
IA -1.66
Br -5.46
LC
LC
B
IA 4.18
Br 0.38
Pe/Pa
IA 3.80
Br 0.00
Pe/Pa
IA 2.98
Br -0.82
Pe/Pa
IA 1.68
Br -2.12
ZI
ZI
IA 0.88
Br -2.92
SN
VTA
SN
IA 0.00
Br -3.80
SN
VTA
SN
IA -0.40
Br -4.20
SN
MnR
SN
IA -1.66
Br -5.46
LC
LC
100
80
60
40
20
0

Fig. 2

A


x axis +45°
1 2 3 4 5 6 7 8 9 10 r
slice

B

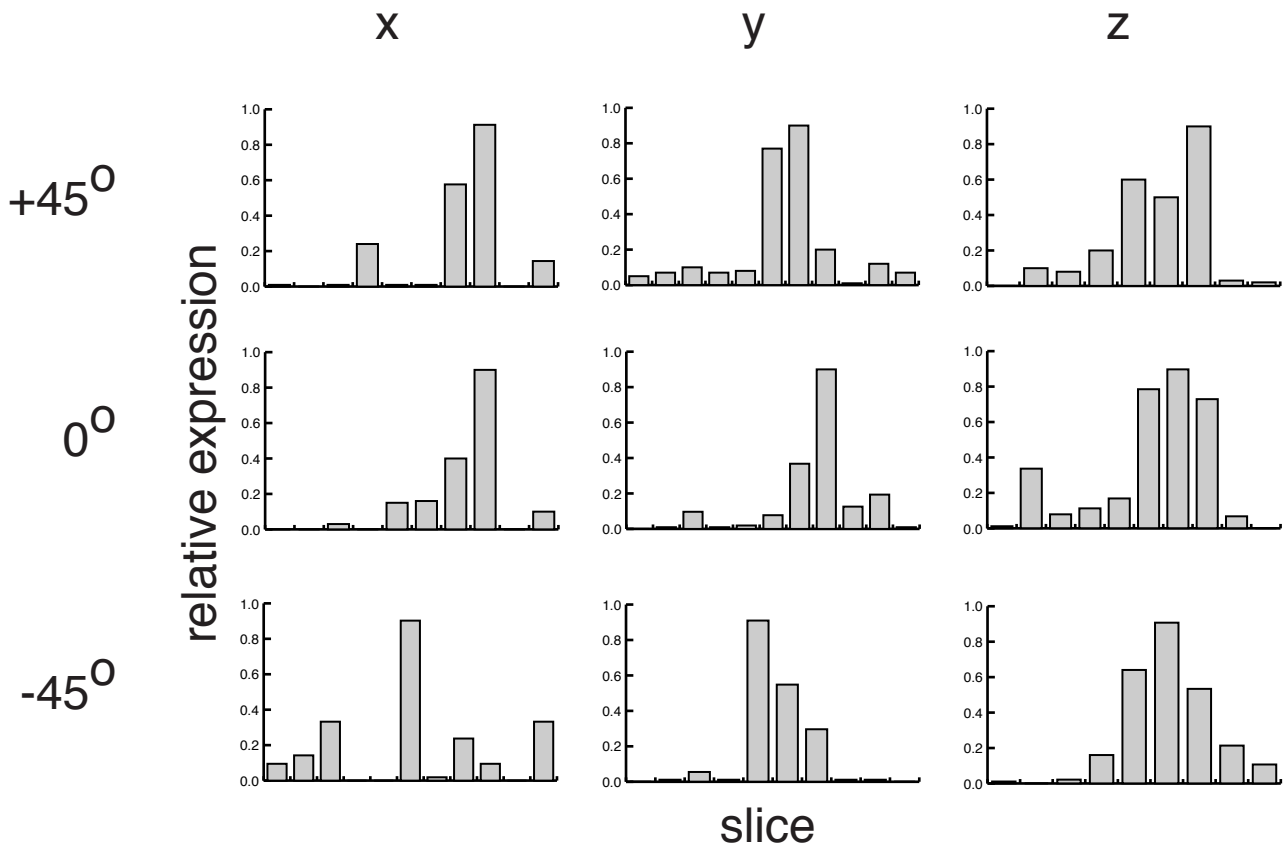
x
y
z
+45°
0°
-45°
relative expression
1.0
0.8
0.6
0.4
0.2
0.0
slice

Fig. 3

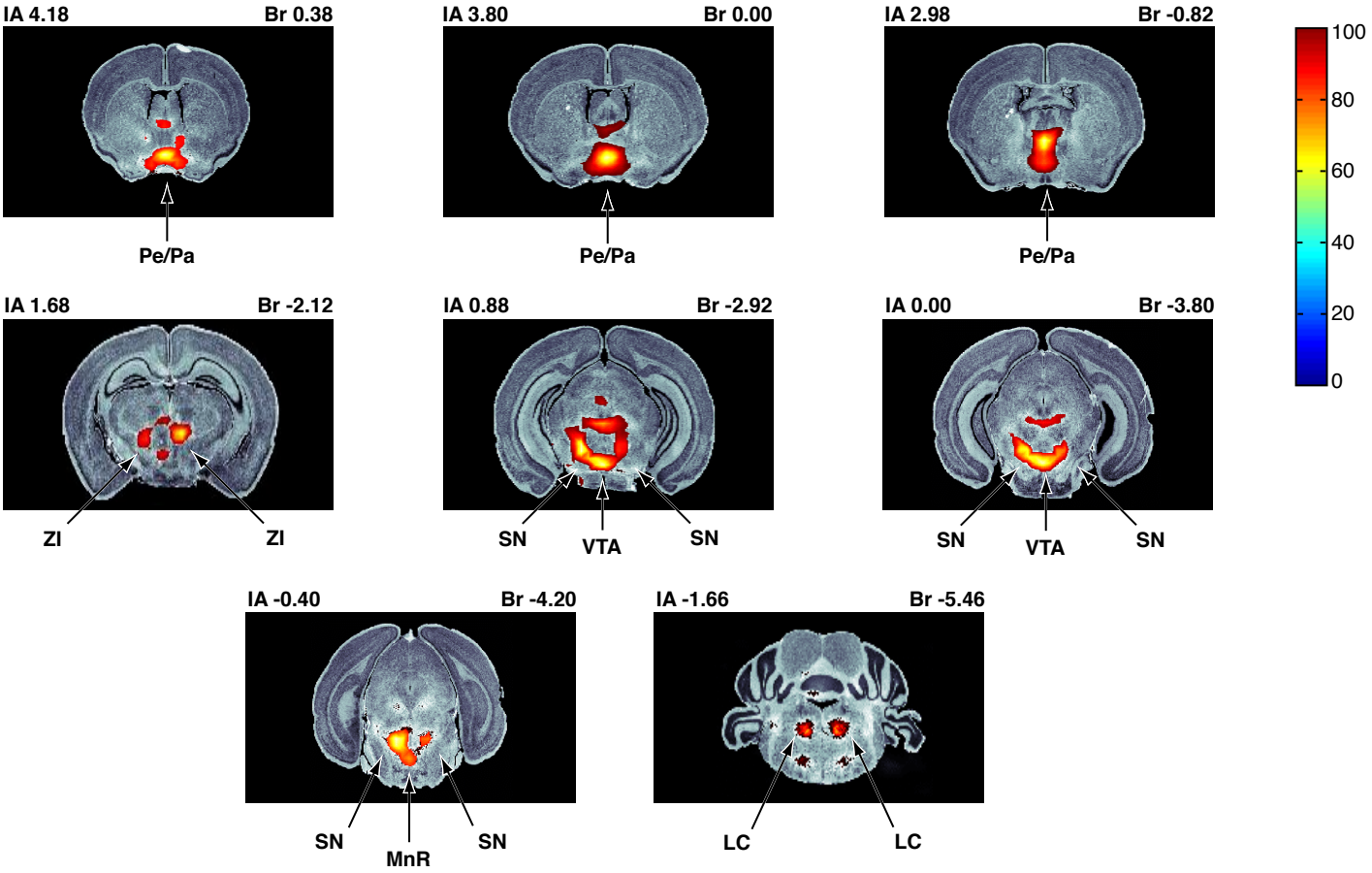
IA 4.18
Br 0.38
Pe/Pa
IA 3.80
Br 0.00
Pe/Pa
IA 2.98
Br -0.82
Pe/Pa
100
80
60
40
20
0
IA 1.68
Br -2.12
ZI
ZI
IA 0.88
Br -2.92
SN
VTA
SN
IA 0.00
Br -3.80
SN
VTA
SN
IA -0.40
Br -4.20
SN
MnR
SN
IA -1.66
Br -5.46
LC
LC

Fig. 4

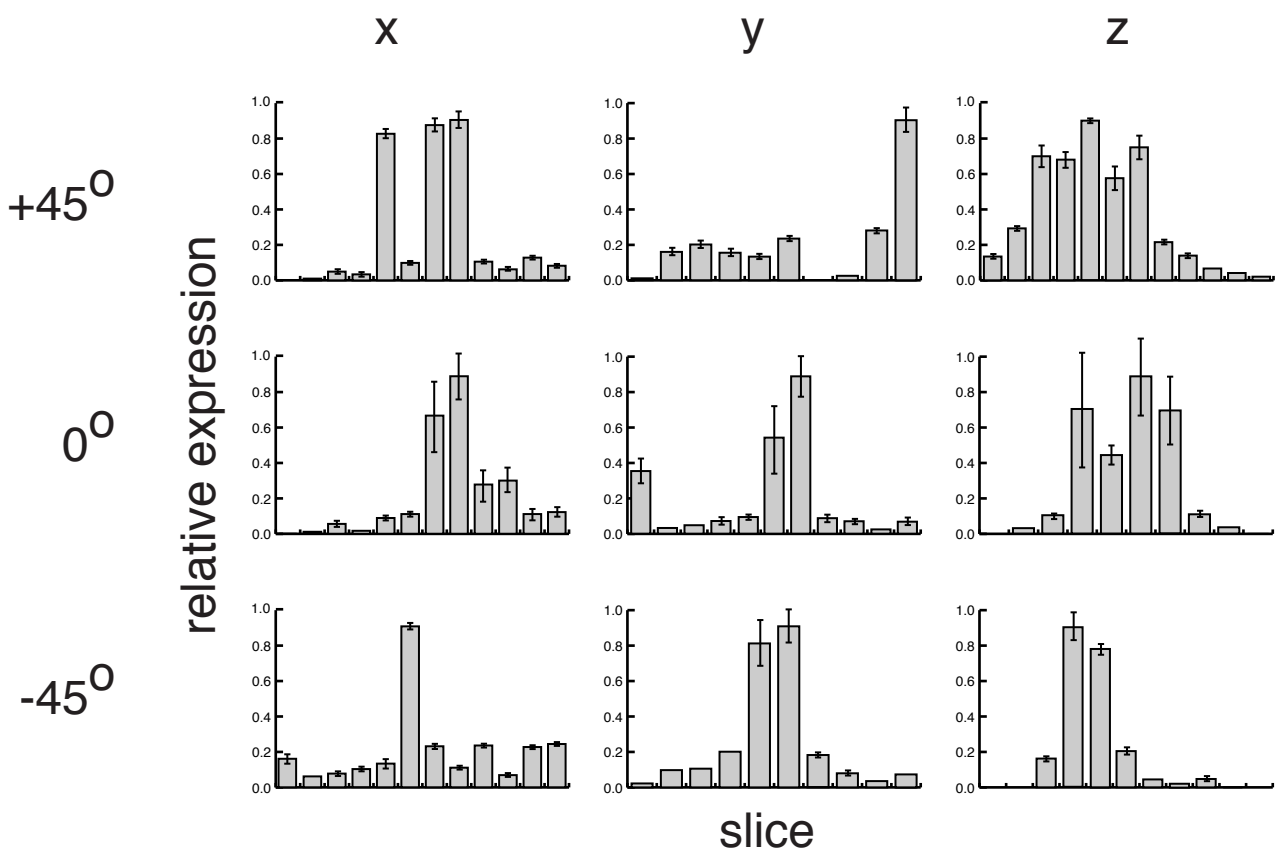

Fig. 5

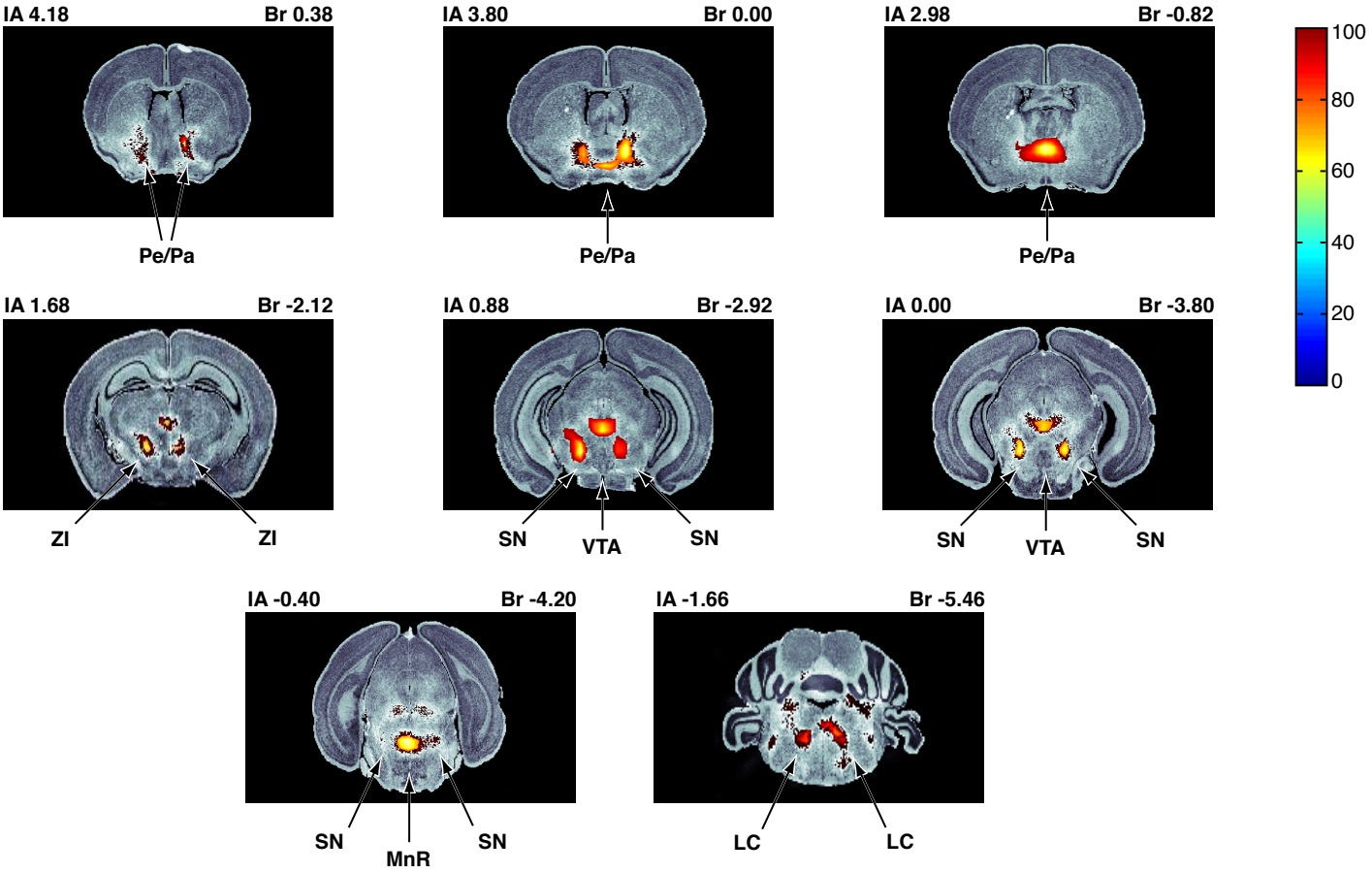
IA 4.18
Br 0.38
Pe/Pa
IA 3.80
Br 0.00
Pe/Pa
IA 2.98
Br -0.82
Pe/Pa
100
80
60
40
20
0
IA 1.68
Br -2.12
ZI
ZI
IA 0.88
Br -2.92
SN
VTA
SN
IA 0.00
Br -3.80
SN
VTA
SN
IA -0.40
Br -4.20
SN
MnR
SN
IA -1.66
Br -5.46
LC
LC

Fig. 6